

## **Steering selectivity in detection of exhaled biomarkers over oxide nanofibers dispersed with noble metals**

Seyeon Park,<sup>a, c</sup> Yunsung Lim,<sup>b</sup> DongHwan Oh,<sup>a</sup> Jaewan Ahn,<sup>a, c</sup> Chungseong Park,<sup>a, c</sup> Minhyun Kim,<sup>a</sup> WooChul Jung,<sup>a</sup> Jihan Kim,<sup>b</sup> and Il-Doo Kim<sup>\*a, c</sup>

a. Department of Materials Science and Engineering, Korea Advanced Institute of Science and Technology (KAIST), 291 Daehak-ro Yuseong-gu Daejeon 34141, Republic of Korea

b. Department of Chemical and Biomolecular Engineering, Korea Advanced Institute of Science and Technology (KAIST), 291 Daehak-ro Yuseong-gu Daejeon 34141, Republic of Korea

c. Membrane Innovation Center for Anti-Virus & Air-Quality Control, KI Nanocentury, KAIST, 291 Daehak-ro Yuseong-gu Daejeon 34141, Republic of Korea

\* Corresponding author.

*E-mail.* idkim@kaist.ac.kr (I.-D. Kim)

## Table of contents

**Figure S1.** (a) XRD patterns and (b) average crystallite sizes of 2Pd-In<sub>2</sub>O<sub>3</sub> nanofibers synthesized from different batches.

**Figure S2.** (a-c) SEM images of 2Pd-In<sub>2</sub>O<sub>3</sub> nanofibers synthesized from different batches.

**Figure S3.** SEM images of In<sub>2</sub>O<sub>3</sub> nanofibers.

**Figure S4.** (a) In 3d and (b) Auger In MNN spectra of In<sub>2</sub>O<sub>3</sub>, 0.05Ru-In<sub>2</sub>O<sub>3</sub>, 0.1Pd-In<sub>2</sub>O<sub>3</sub>, and 2Pt-In<sub>2</sub>O<sub>3</sub> samples.

**Figure S5.** Gas sensing results at controllable loading of (a) Ru-In<sub>2</sub>O<sub>3</sub>, (b) Pd-In<sub>2</sub>O<sub>3</sub>, and (c) Pt-In<sub>2</sub>O<sub>3</sub> respectively toward 5 ppm CH<sub>3</sub>SH, H<sub>2</sub>S, and CH<sub>3</sub>COCH<sub>3</sub> at various temperatures.

**Table S1.** Physical characteristics of In<sub>2</sub>O<sub>3</sub>, 0.05Ru-In<sub>2</sub>O<sub>3</sub>, 0.1Pd-In<sub>2</sub>O<sub>3</sub>, and 2Pt-In<sub>2</sub>O<sub>3</sub> samples.

**Figure S6.** Repeatability tests results of (a) dynamic resistance change and (b) dynamic response during sensing tests toward 1–5 ppm H<sub>2</sub>S.

**Figure S7.** XRD patterns of Ru-, Pd-, and Pt-In<sub>2</sub>O<sub>3</sub> samples.

**Figure S8.** Synchrotron XRD patterns of the pristine In<sub>2</sub>O<sub>3</sub>, 0.05Ru-In<sub>2</sub>O<sub>3</sub>, 0.1Pd-In<sub>2</sub>O<sub>3</sub>, and 2Pt-In<sub>2</sub>O<sub>3</sub> samples.

**Figure S9.** Average crystallite sizes, calculated by the Scherrer equation for (222), (400), and (440) reflections, of the pristine In<sub>2</sub>O<sub>3</sub>, 0.05Ru-In<sub>2</sub>O<sub>3</sub>, 0.1Pd-In<sub>2</sub>O<sub>3</sub>, and 2Pt-In<sub>2</sub>O<sub>3</sub> samples.

**Figure S10.** BJH pore size distribution of In<sub>2</sub>O<sub>3</sub>, 0.05Ru-In<sub>2</sub>O<sub>3</sub>, 0.1Pd-In<sub>2</sub>O<sub>3</sub>, and 2Pt-In<sub>2</sub>O<sub>3</sub> samples.

**Figure S11.** The deconvolution results O 1s spectra obtained from XPS analysis for (a) In<sub>2</sub>O<sub>3</sub>, (b) 0.05Ru-In<sub>2</sub>O<sub>3</sub>, (c) 0.1Pd-In<sub>2</sub>O<sub>3</sub>, and (d) 2Pt-In<sub>2</sub>O<sub>3</sub> samples.

**Figure S12.** In<sub>2</sub>O<sub>3</sub> lattice constants of various samples, calculated from the synchrotron XRD results.

**Figure S13.** UPS spectra, cut-off energy estimation, and fermi level estimation of (a-c) In<sub>2</sub>O<sub>3</sub>, (d-f) 0.05Ru-In<sub>2</sub>O<sub>3</sub>, (g-i) 0.1Pd-In<sub>2</sub>O<sub>3</sub>, and (j-l) 2Pt-In<sub>2</sub>O<sub>3</sub> samples.

**Figure S14.** Configurations of CH<sub>3</sub>SH adsorbed onto (a, b, c, d) Ru-In<sub>2</sub>O<sub>3</sub>, (e, f) comparison of the calculated values of the adsorption energy and the charge transfer.

**Figure S15.** Configurations of CH<sub>3</sub>SH adsorbed onto (a, b, c, d) Pd-In<sub>2</sub>O<sub>3</sub>, (e, f) comparison of the calculated values of the adsorption energy and the charge transfer.

**Figure S16.** Configurations of CH<sub>3</sub>SH adsorbed onto (a, b, c, d) Pt-In<sub>2</sub>O<sub>3</sub>, (e, f) comparison of the calculated values of the adsorption energy and the charge transfer.

**Figure S17.** Configurations of H<sub>2</sub>S adsorbed onto (a, b, c, d) Ru-In<sub>2</sub>O<sub>3</sub>, (e, f) comparison of

the calculated values of the adsorption energy and the charge transfer.

**Figure S18.** Configurations of H<sub>2</sub>S adsorbed onto (a, b, c, d) Pd-In<sub>2</sub>O<sub>3</sub>, (e, f) comparison of the calculated values of the adsorption energy and the charge transfer.

**Figure S19.** Configurations of H<sub>2</sub>S adsorbed onto (a, b, c, d) Pt-In<sub>2</sub>O<sub>3</sub>, (e, f) comparison of the calculated values of the adsorption energy and the charge transfer.

**Figure S20.** Configurations of CH<sub>3</sub>COCH<sub>3</sub> adsorbed onto (a, b, c, d) Ru-In<sub>2</sub>O<sub>3</sub>, (e, f) comparison of the calculated values of the adsorption energy and the charge transfer.

**Figure S21.** Configurations of CH<sub>3</sub>COCH<sub>3</sub> adsorbed onto (a, b, c, d) Pd-In<sub>2</sub>O<sub>3</sub>, (e, f) comparison of the calculated values of the adsorption energy and the charge transfer.

**Figure S22.** Configurations of CH<sub>3</sub>COCH<sub>3</sub> adsorbed onto (a, b, c, d) Pt-In<sub>2</sub>O<sub>3</sub>, (e, f) comparison of the calculated values of the adsorption energy and the charge transfer.

**Table S2.** The computation results of the adsorption energy and the charge transfer values between CH<sub>3</sub>SH gas and metal atoms. (Bold texts indicate the optimized configuration.)

**Table S3.** The computation results of the adsorption energy and the charge transfer values between H<sub>2</sub>S gas and metal atoms. (Bold texts indicate the optimized configuration.)

**Table S4.** The computation results of the adsorption energy and the charge transfer values between CH<sub>3</sub>SOCH<sub>3</sub> gas and metal atoms. (Bold texts indicate the optimized configuration.)

**Table S5.** The computation results of the adsorption energy, the charge transfer values and the distance between metals and gases. (Bold texts indicate the most favorable sensing materials toward each analyte.)

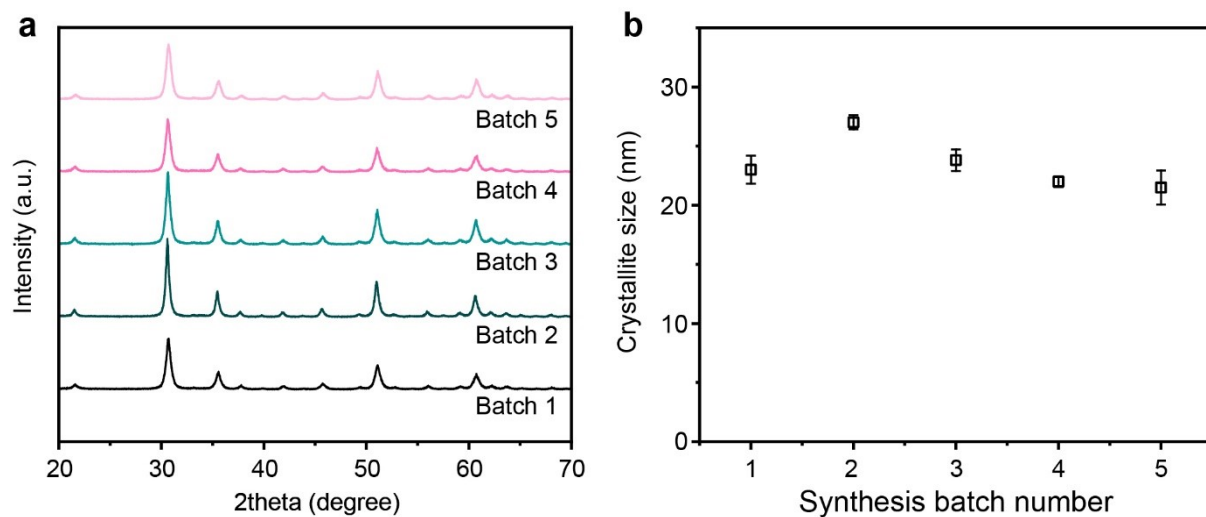


**Figure S1.** (a) XRD patterns and (b) average crystallite sizes of 2Pd-In<sub>2</sub>O<sub>3</sub> nanofibers synthesized from different batches.

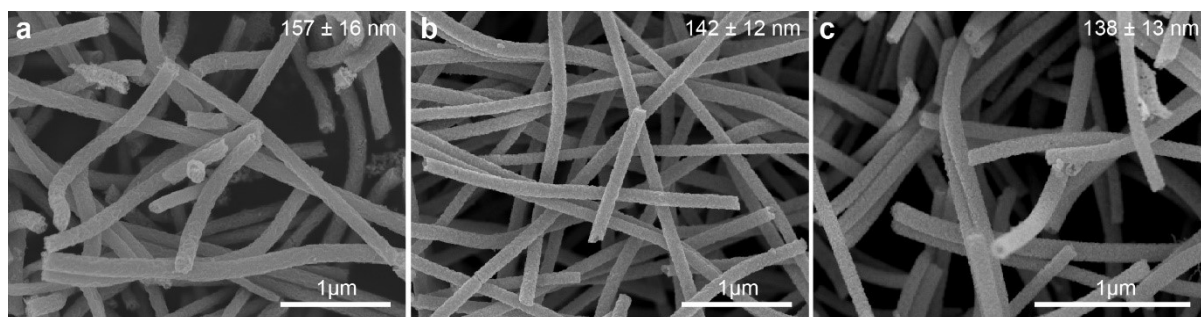


**Figure S2.** (a-c) SEM images of 2Pd-In<sub>2</sub>O<sub>3</sub> nanofibers synthesized from different batches.

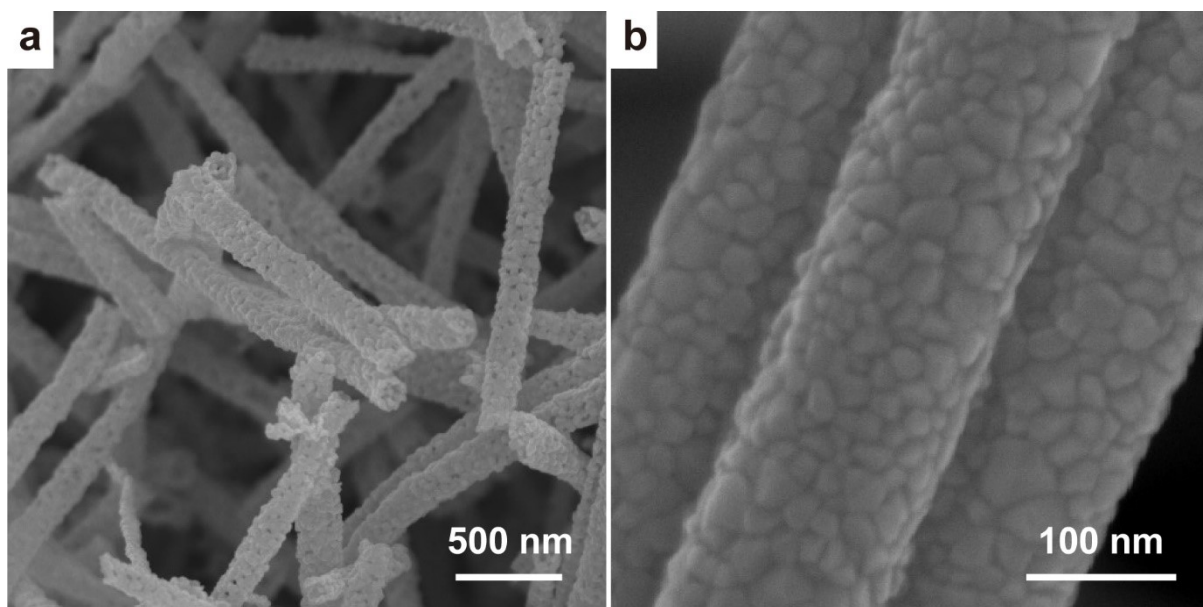


**Figure S3.** SEM images of  $\text{In}_2\text{O}_3$  nanofibers.

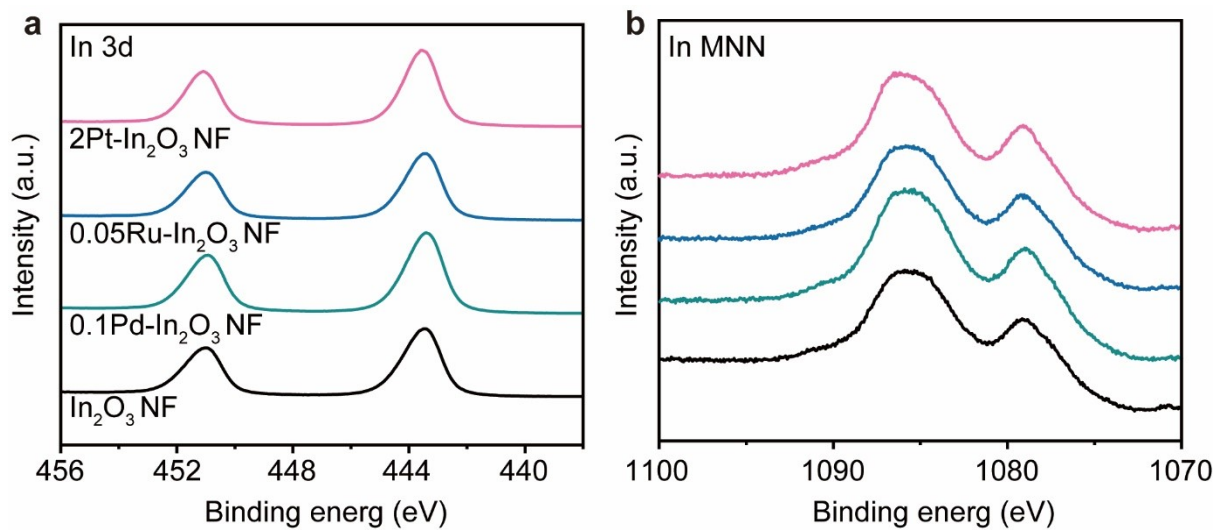


**Figure S4.** (a) In 3d and (b) Auger In MNN spectra of  $\text{In}_2\text{O}_3$ ,  $0.05\text{Ru-In}_2\text{O}_3$ ,  $0.1\text{Pd-In}_2\text{O}_3$ , and  $2\text{Pt-In}_2\text{O}_3$  samples.

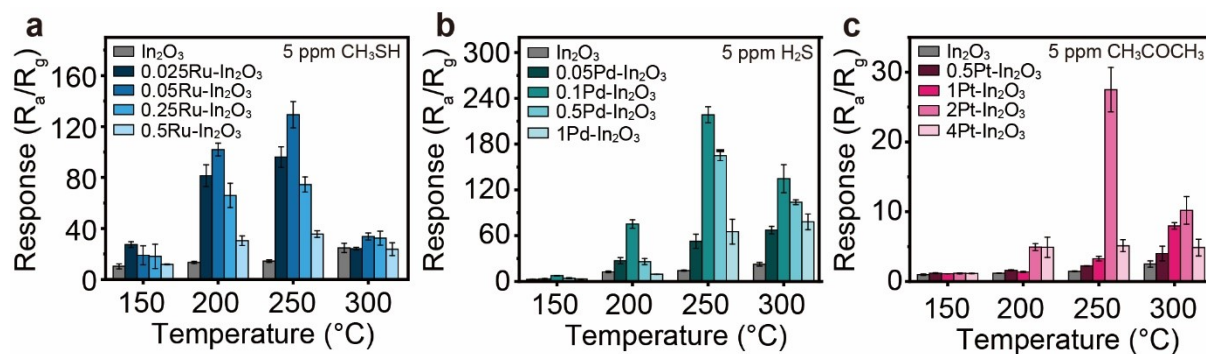


**Figure S5.** Gas sensing results at controllable loading of (a) Ru- $\text{In}_2\text{O}_3$ , (b) Pd- $\text{In}_2\text{O}_3$ , and (c) Pt- $\text{In}_2\text{O}_3$  respectively toward 5 ppm  $\text{CH}_3\text{SH}$ ,  $\text{H}_2\text{S}$ , and  $\text{CH}_3\text{COCH}_3$  at various temperatures.

Sample	Noble metal loading <sup>[a]</sup> (wt%)	$D_{\text{In-XRD}}$ <sup>[b]</sup> (nm)	$S_{\text{BET}}$ <sup>[c]</sup> ( $\text{m}^2 \text{g}^{-1}$ )	$V_{\text{pore}}$ <sup>[c]</sup> ( $\text{cm}^3 \text{g}^{-1}$ )
$\text{In}_2\text{O}_3$		$25.2 \pm 1.3$	11	0.041
0.05Ru- $\text{In}_2\text{O}_3$	0.04	$23.2 \pm 0.8$	14	0.055
0.1Pd- $\text{In}_2\text{O}_3$	0.08	$23.5 \pm 0.8$	15	0.057
2Pt- $\text{In}_2\text{O}_3$	1.9	$17.1 \pm 0.9$	28	0.108

**Table S1.** Physical characteristics of  $\text{In}_2\text{O}_3$ , 0.05Ru- $\text{In}_2\text{O}_3$ , 0.1Pd- $\text{In}_2\text{O}_3$ , and 2Pt- $\text{In}_2\text{O}_3$  samples. [a] Noble metal loading based on wt% (Metal/ $\text{In}_2\text{O}_3$ ) was measured by ICP-MS, [b] average crystallite size of  $\text{In}_2\text{O}_3$  (222), (400), (440) and (622) reflections were calculated by the Scherrer equation, and [c] BET surface area ( $S_{\text{BET}}$ ) and pore volume ( $V_{\text{pore}}$ ) of the oxides were obtained from  $\text{N}_2$  physisorption at  $-196^\circ\text{C}$ .

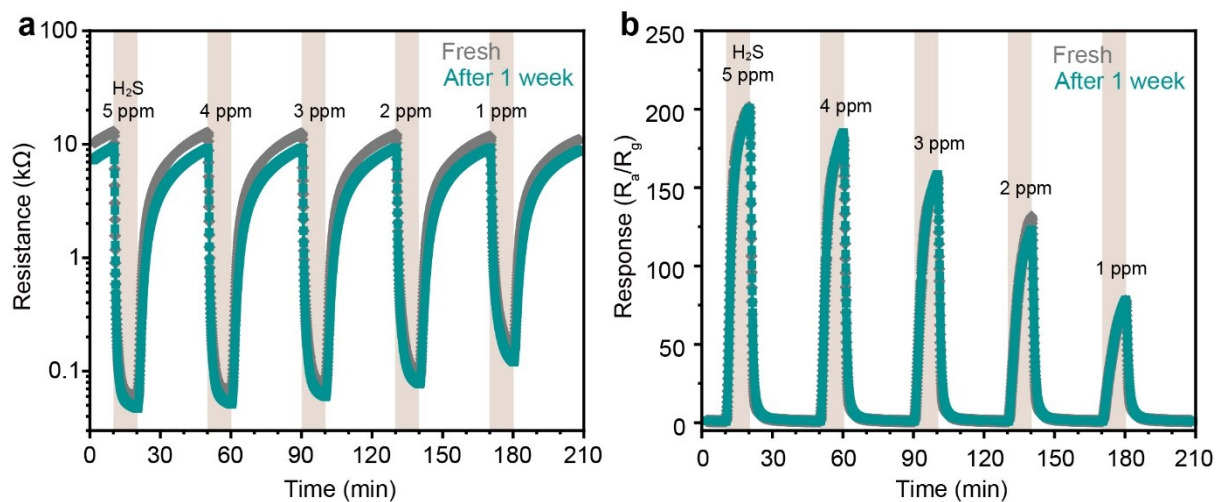


**Figure S6.** Repeatability tests results of (a) dynamic resistance change and (b) dynamic response during sensing tests toward 1–5 ppm H<sub>2</sub>S.

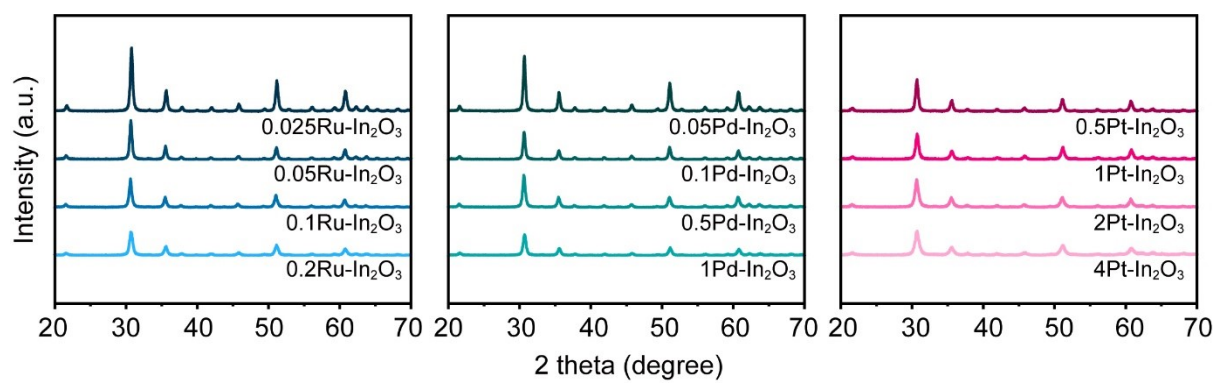


**Figure S7.** XRD patterns of Ru-, Pd-, and Pt-In<sub>2</sub>O<sub>3</sub> samples.

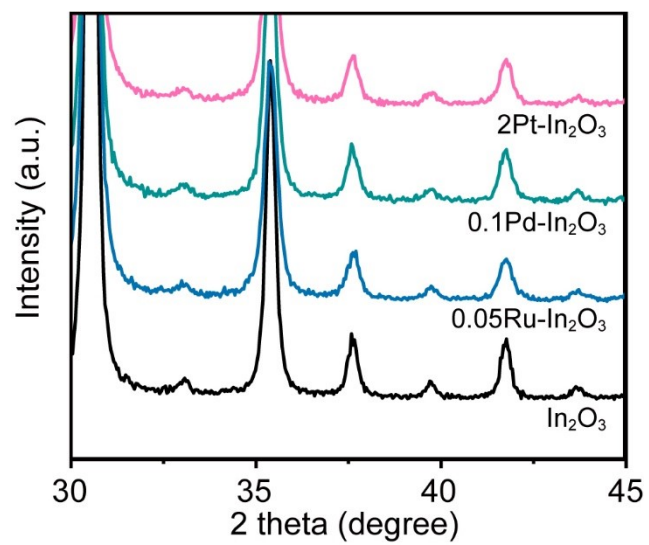


**Figure S8.** Synchrotron XRD patterns of the pristine In<sub>2</sub>O<sub>3</sub>, 0.05Ru- In<sub>2</sub>O<sub>3</sub>, 0.1Pd- In<sub>2</sub>O<sub>3</sub>, and 2Pt-In<sub>2</sub>O<sub>3</sub> samples.

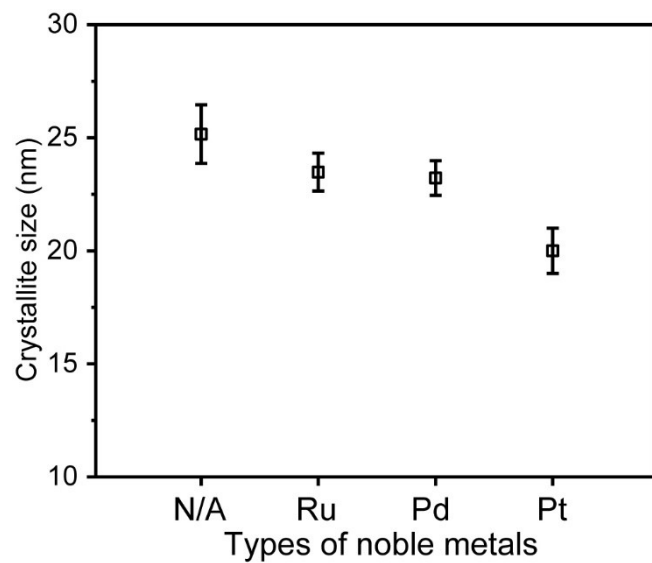


**Figure S9.** Average crystallite sizes, calculated by the Scherrer equation for (222), (400), and (440) reflections, of the pristine  $\text{In}_2\text{O}_3$ , 0.05Ru-  $\text{In}_2\text{O}_3$ , 0.1Pd-  $\text{In}_2\text{O}_3$ , and 2Pt- $\text{In}_2\text{O}_3$  samples.

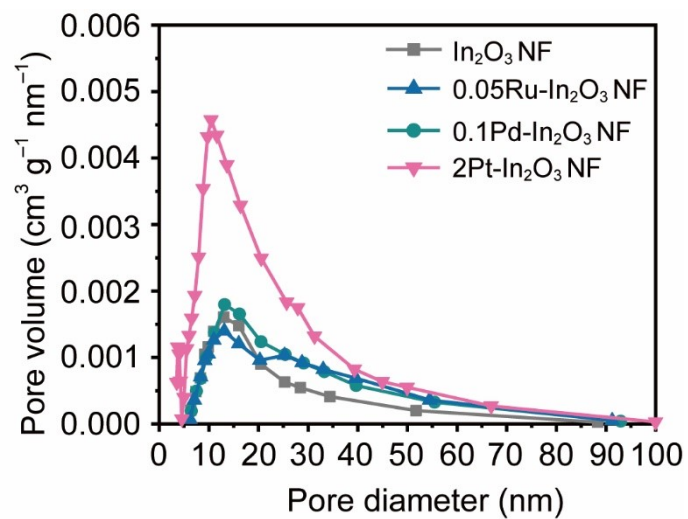


**Figure S10.** BJH pore size distribution of In<sub>2</sub>O<sub>3</sub>, 0.05Ru-In<sub>2</sub>O<sub>3</sub>, 0.1Pd-In<sub>2</sub>O<sub>3</sub>, and 2Pt-In<sub>2</sub>O<sub>3</sub> samples.

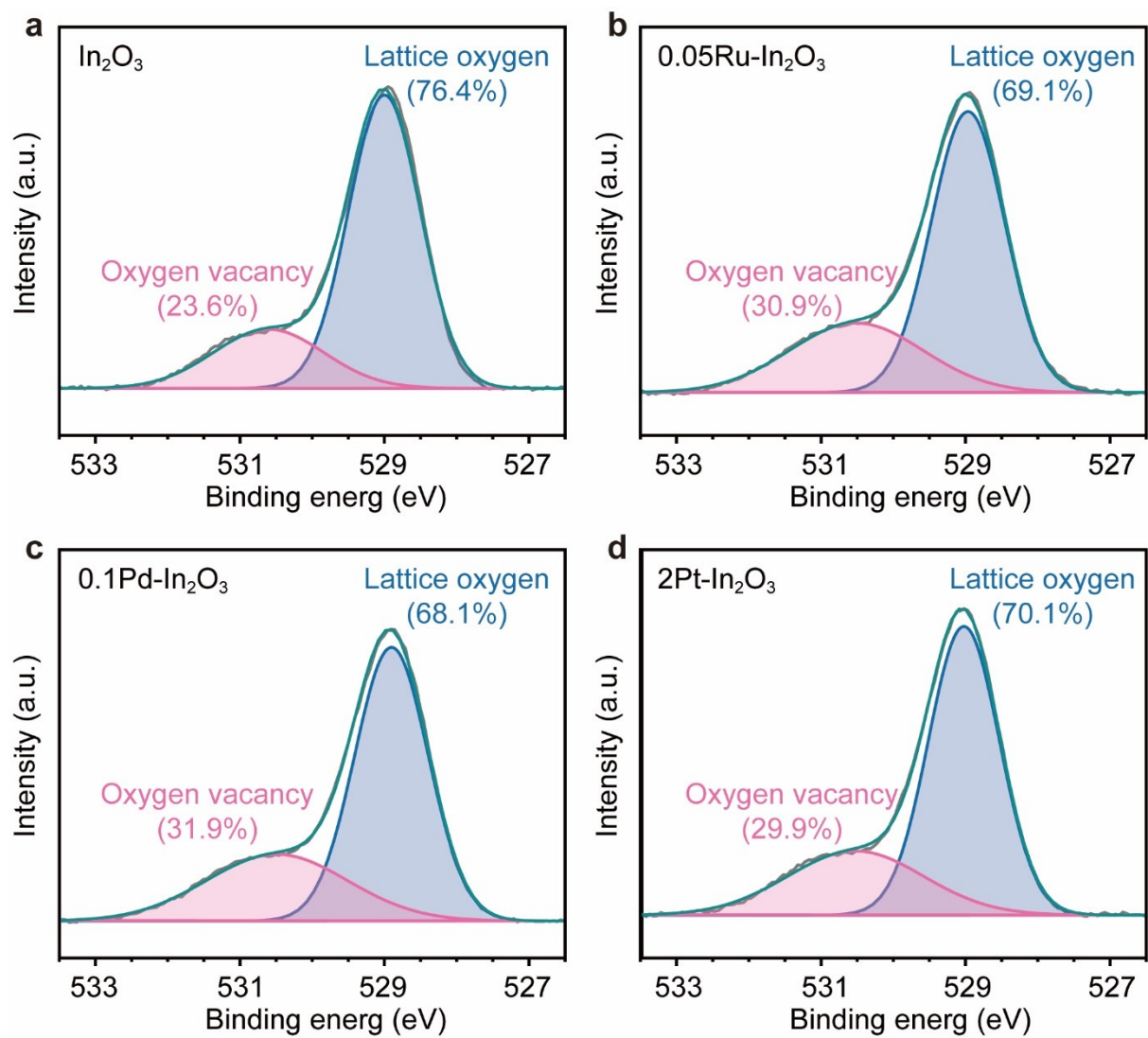


**Figure S11.** The deconvolution results O 1s spectra obtained from XPS analysis for (a)  $\text{In}_2\text{O}_3$ , (b)  $0.05\text{Ru-In}_2\text{O}_3$ , (c)  $0.1\text{Pd-In}_2\text{O}_3$ , and (d)  $2\text{Pt-In}_2\text{O}_3$  samples.

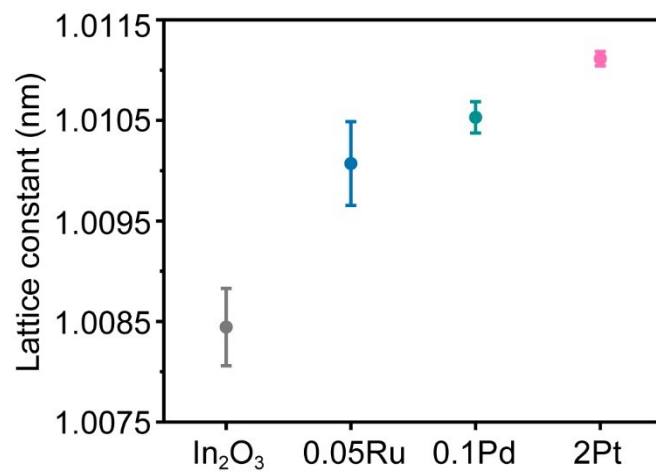


**Figure S12.** In<sub>2</sub>O<sub>3</sub> lattice constants of various samples, calculated from the synchrotron XRD results.

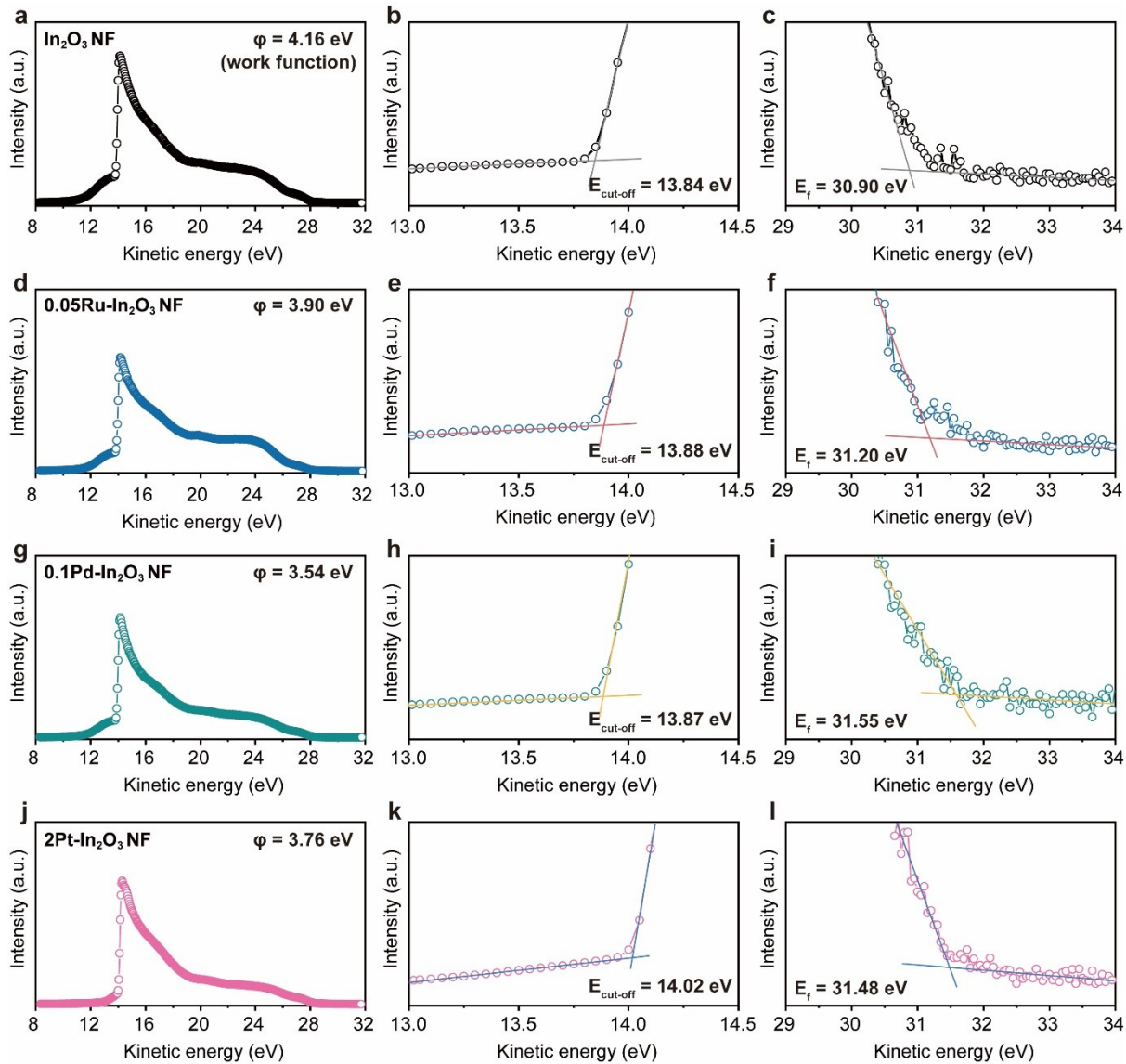


**Figure S13.** UPS spectra, cut-off energy estimation, and fermi level estimation of (a-c)  $\text{In}_2\text{O}_3$ , (d-f) 0.05Ru-  $\text{In}_2\text{O}_3$ , (g-i) 0.1Pd-  $\text{In}_2\text{O}_3$ , and (j-l) 2Pt- $\text{In}_2\text{O}_3$  samples.

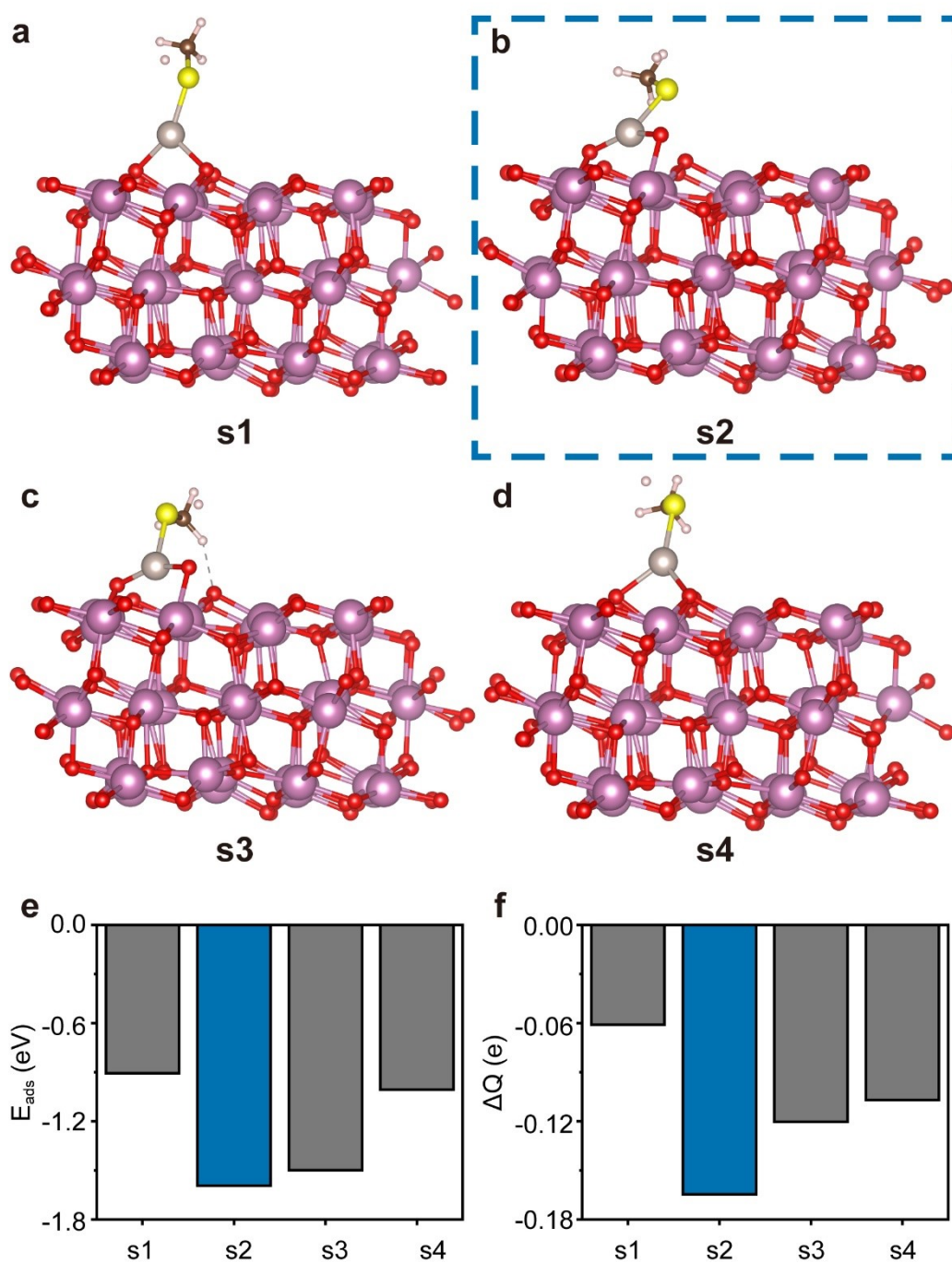


**Figure S14.** Configurations of CH<sub>3</sub>SH adsorbed onto (a, b, c, d) Ru-In<sub>2</sub>O<sub>3</sub>, (e, f) comparison of the calculated values of the adsorption energy and the charge transfer.

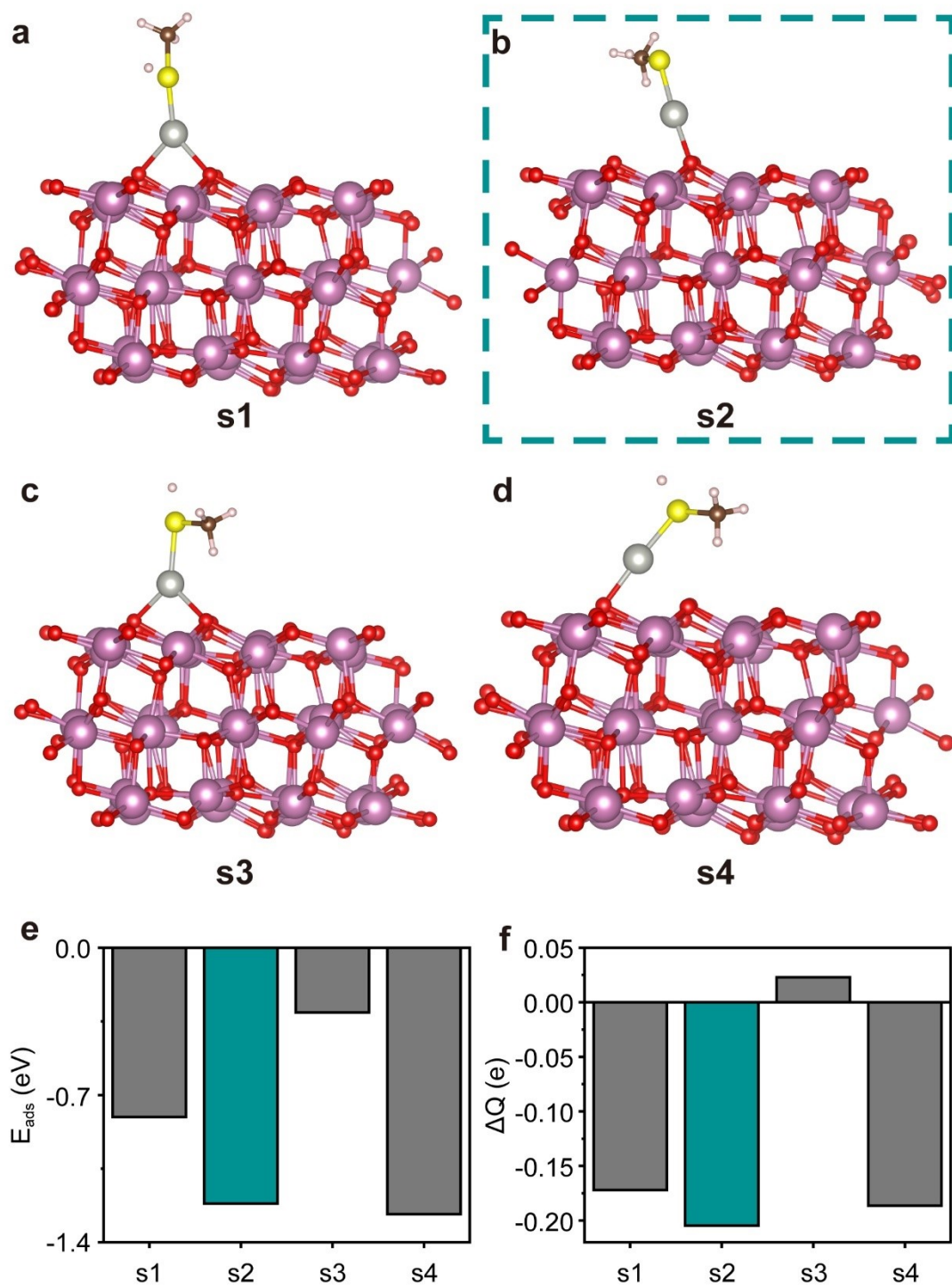


**Figure S15.** Configurations of CH<sub>3</sub>SH adsorbed onto (a, b, c, d) Pd-In<sub>2</sub>O<sub>3</sub>, (e, f) comparison of the calculated values of the adsorption energy and the charge transfer.

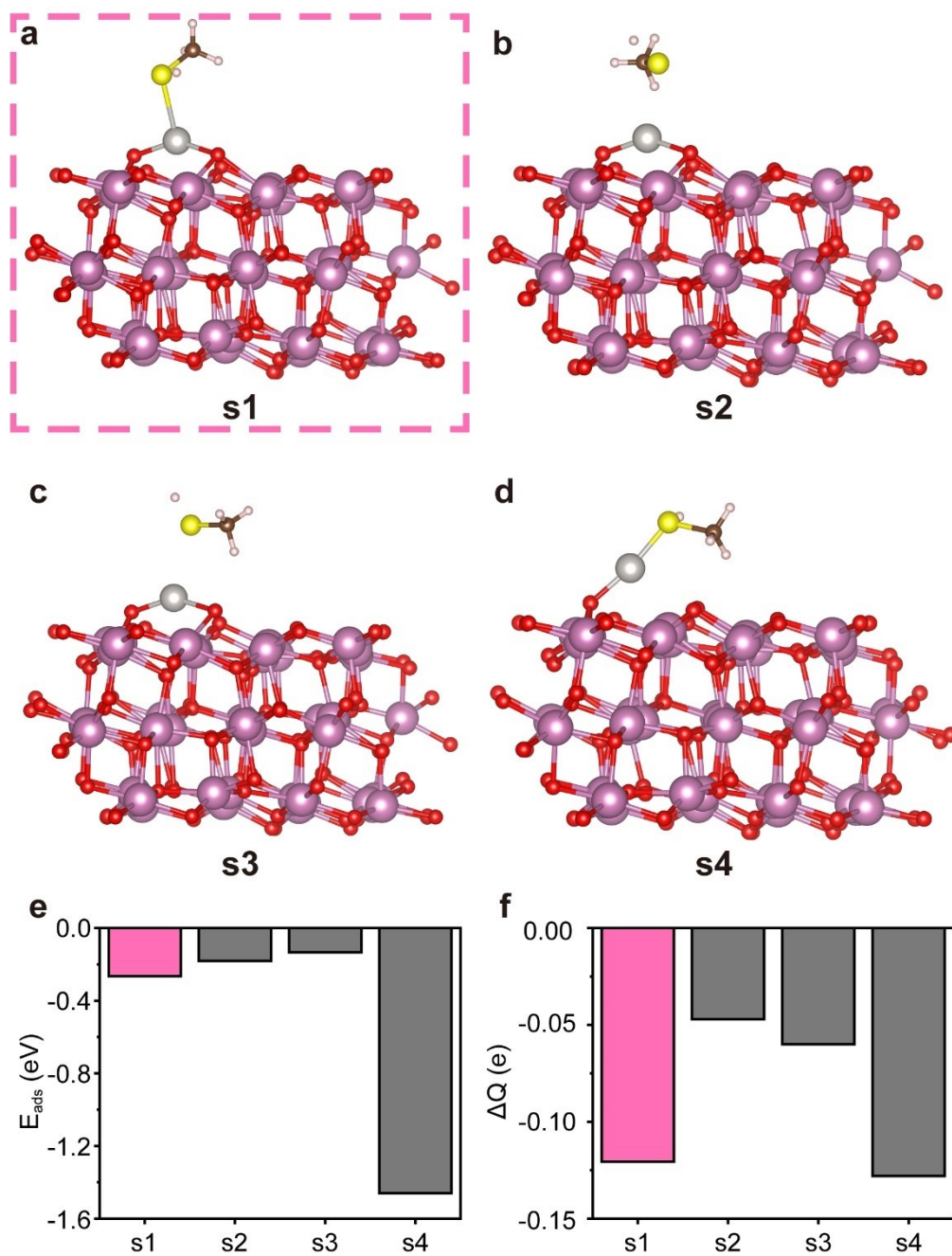


**Figure S16.** Configurations of CH<sub>3</sub>SH adsorbed onto (a, b, c, d) Pt-In<sub>2</sub>O<sub>3</sub>, (e, f) comparison of the calculated values of the adsorption energy and the charge transfer.

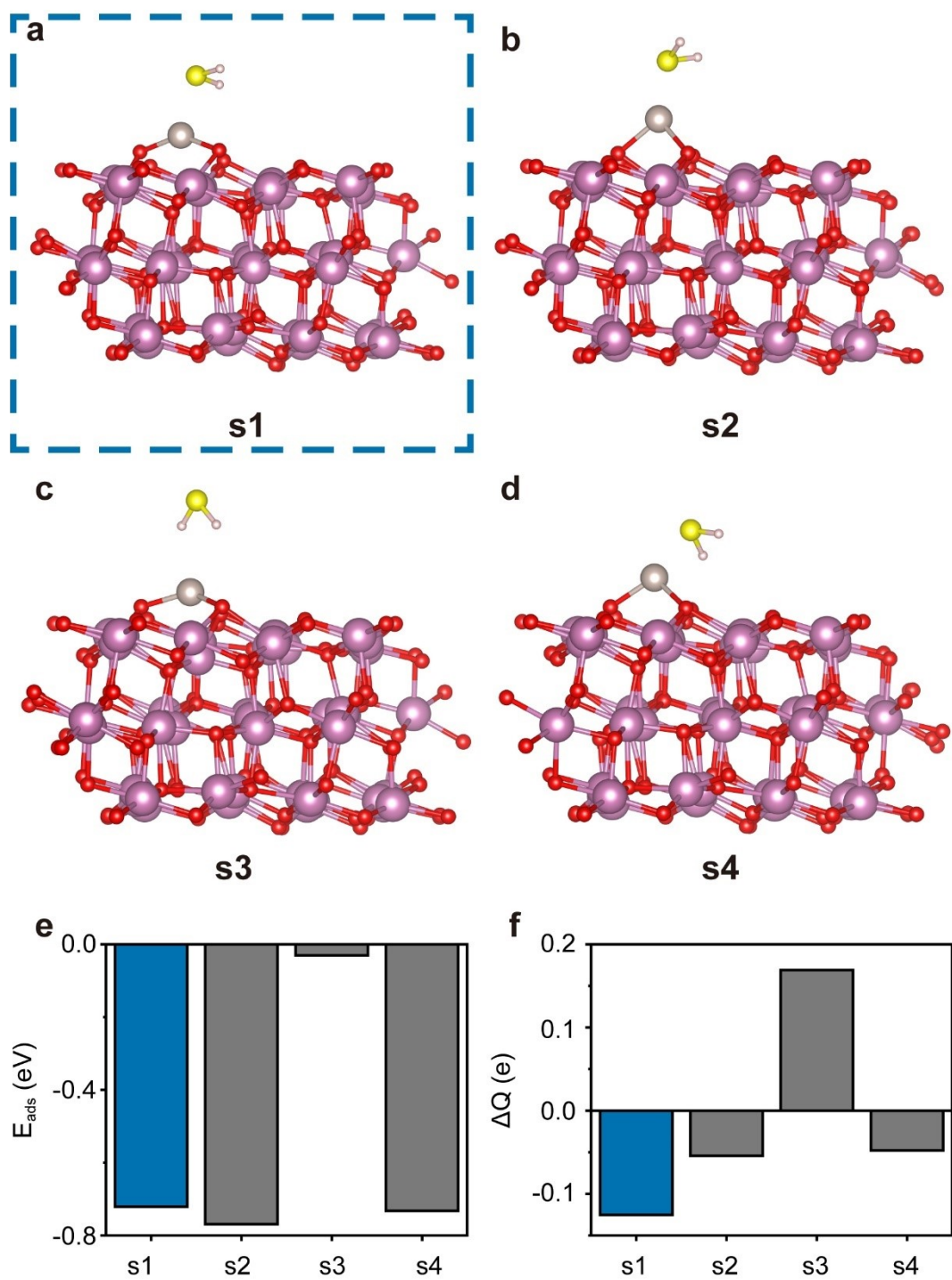


**Figure S17.** Configurations of H<sub>2</sub>S adsorbed onto (a, b, c, d) Ru-In<sub>2</sub>O<sub>3</sub>, (e, f) comparison of the calculated values of the adsorption energy and the charge transfer.

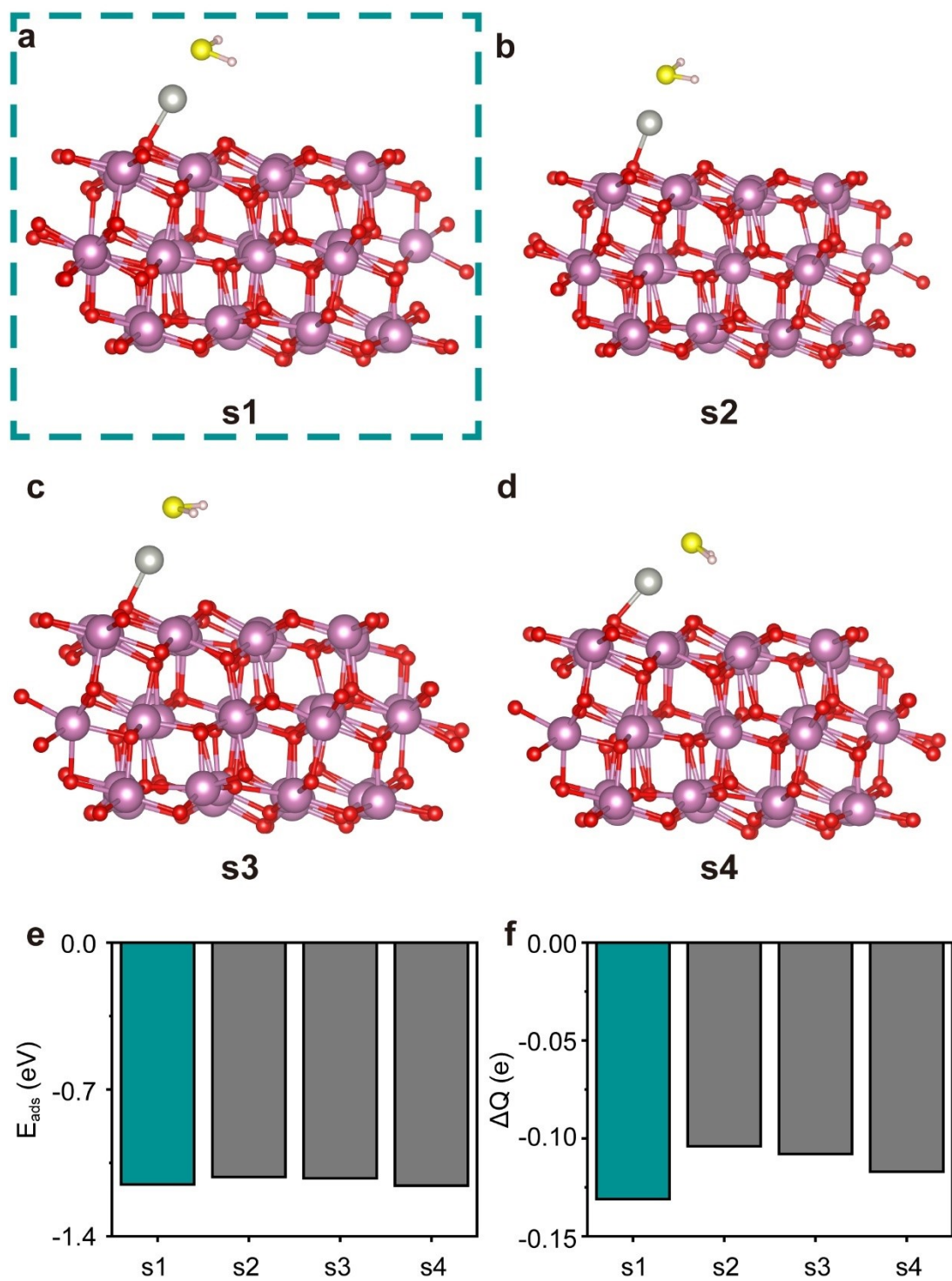


**Figure S18.** Configurations of H<sub>2</sub>S adsorbed onto (a, b, c, d) Pd-In<sub>2</sub>O<sub>3</sub>, (e, f) comparison of the calculated values of the adsorption energy and the charge transfer.

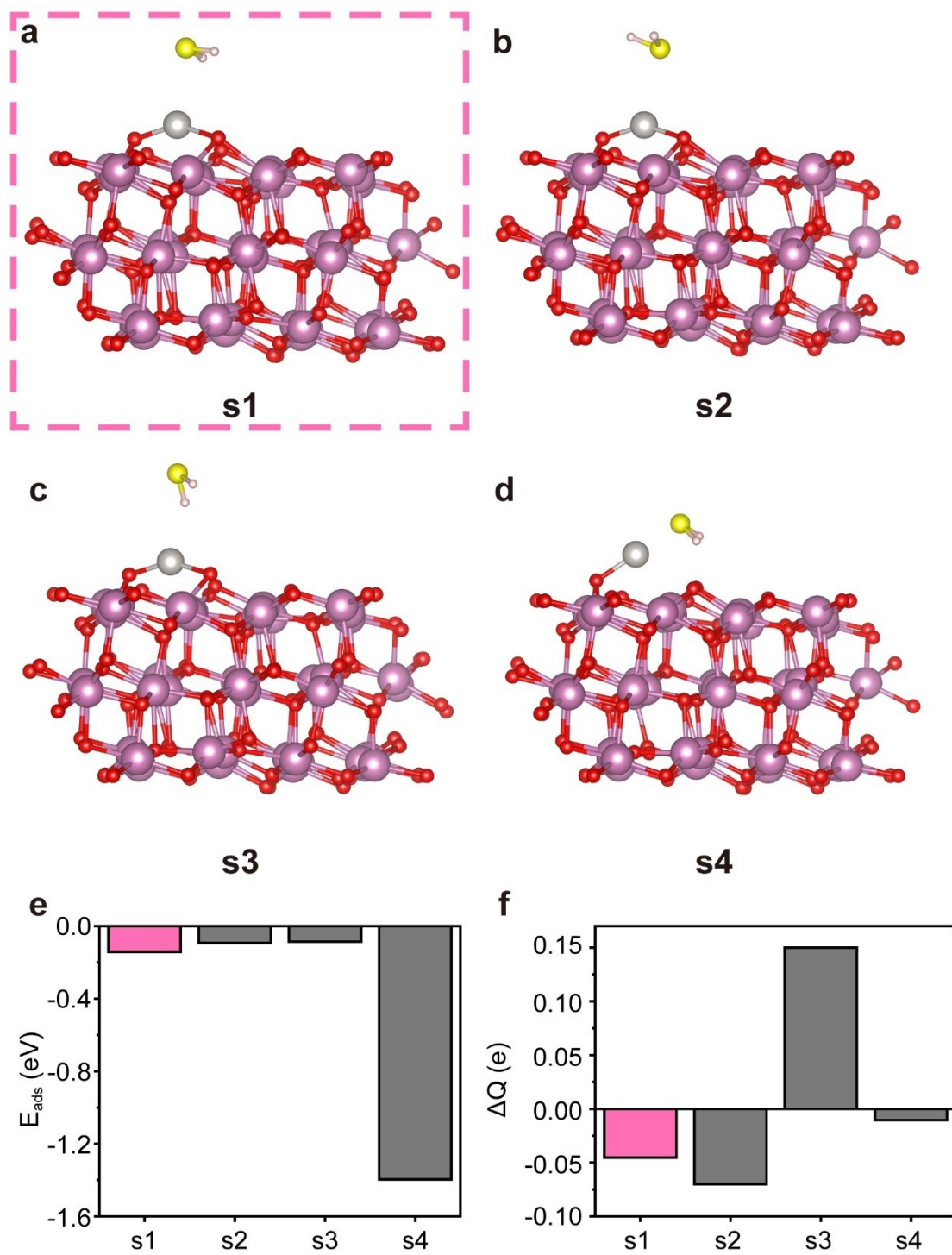


**Figure S19.** Configurations of H<sub>2</sub>S adsorbed onto (a, b, c, d) Pt-In<sub>2</sub>O<sub>3</sub>, (e, f) comparison of the calculated values of the adsorption energy and the charge transfer.

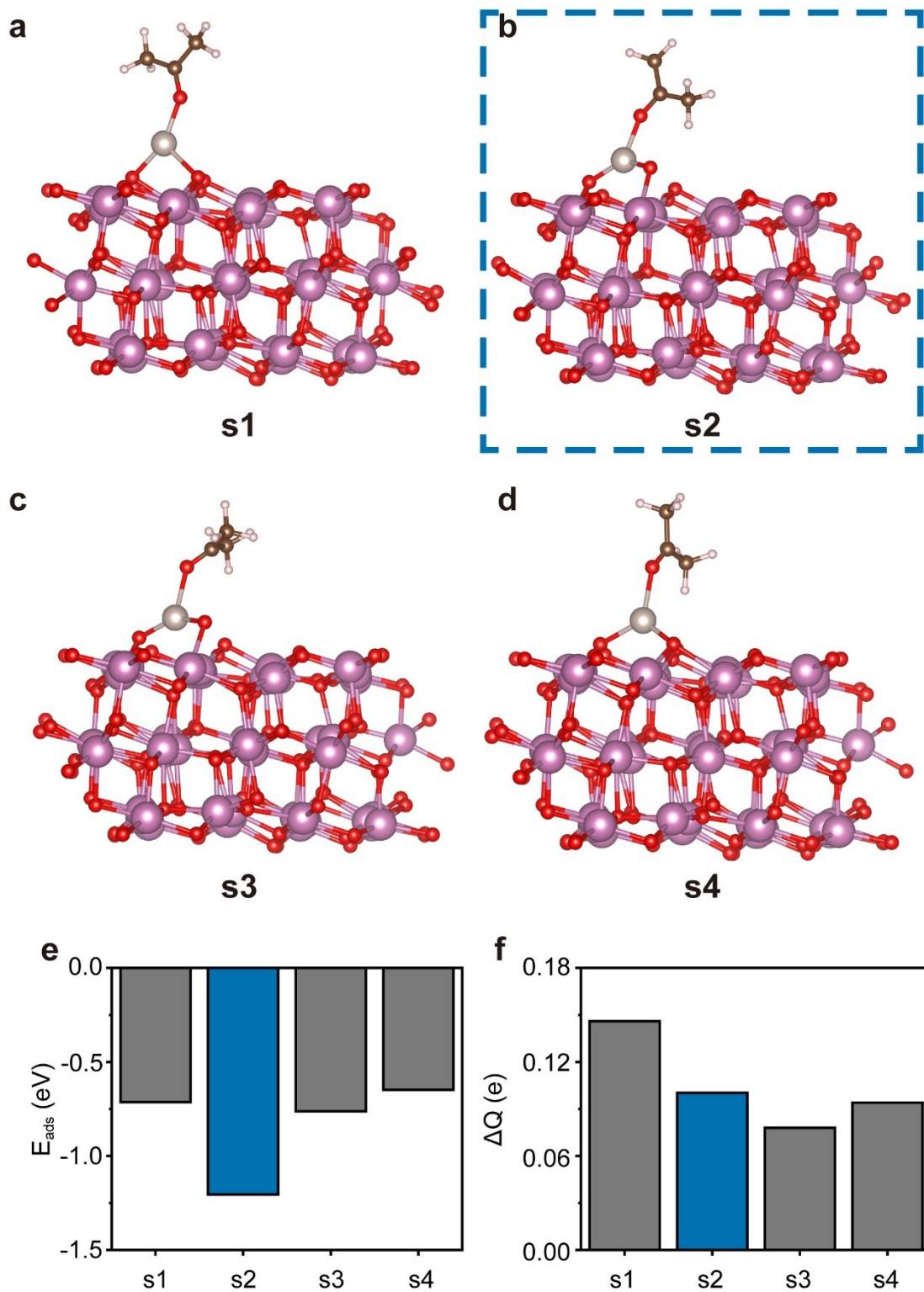


**Figure S20.** Configurations of  $\text{CH}_3\text{COCH}_3$  adsorbed onto (a, b, c, d)  $\text{Ru-In}_2\text{O}_3$ , (e, f) comparison of the calculated values of the adsorption energy and the charge transfer.

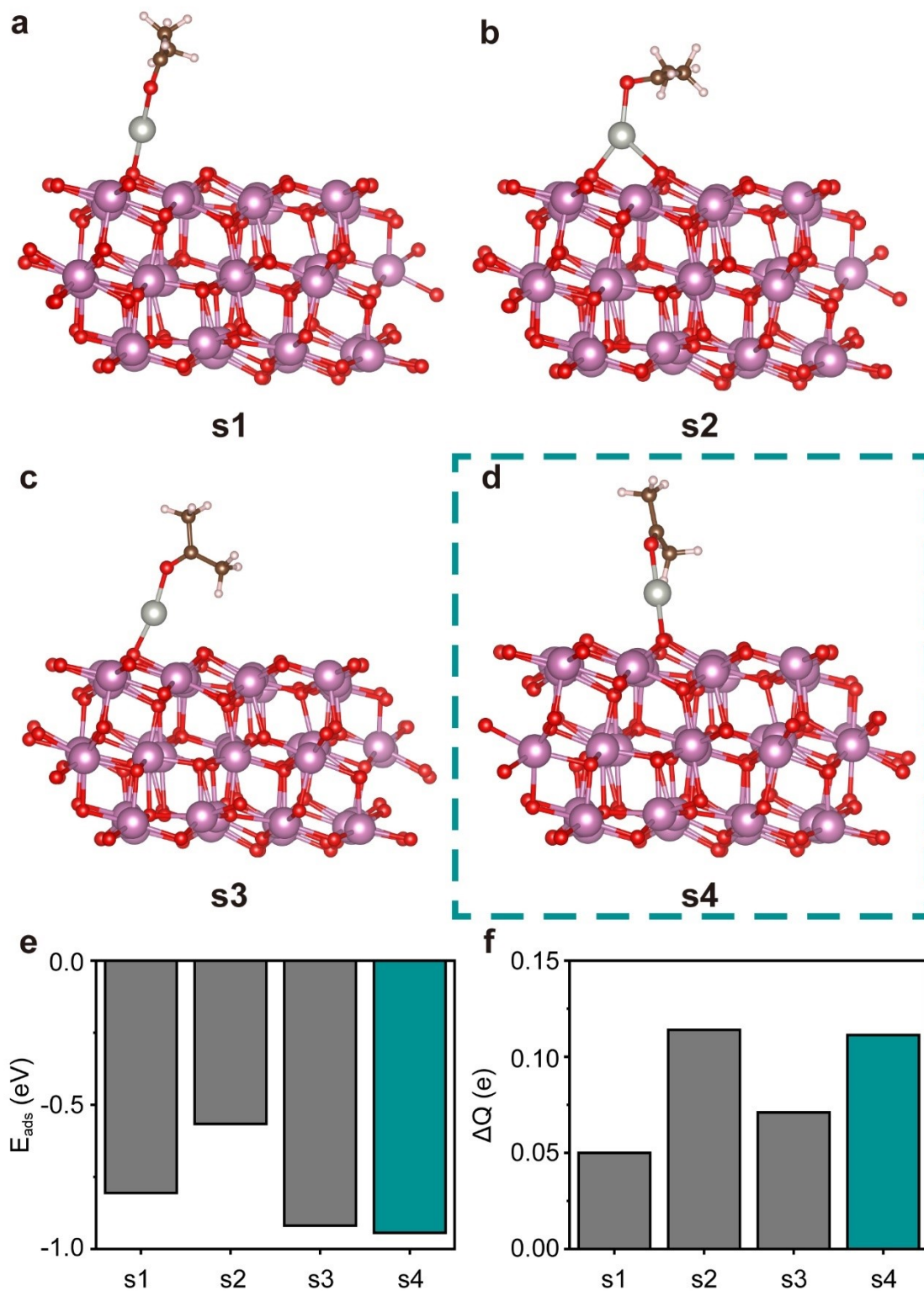


**Figure S21.** Configurations of  $\text{CH}_3\text{COCH}_3$  adsorbed onto (a, b, c, d)  $\text{Pd-In}_2\text{O}_3$ , (e, f) comparison of the calculated values of the adsorption energy and the charge transfer.

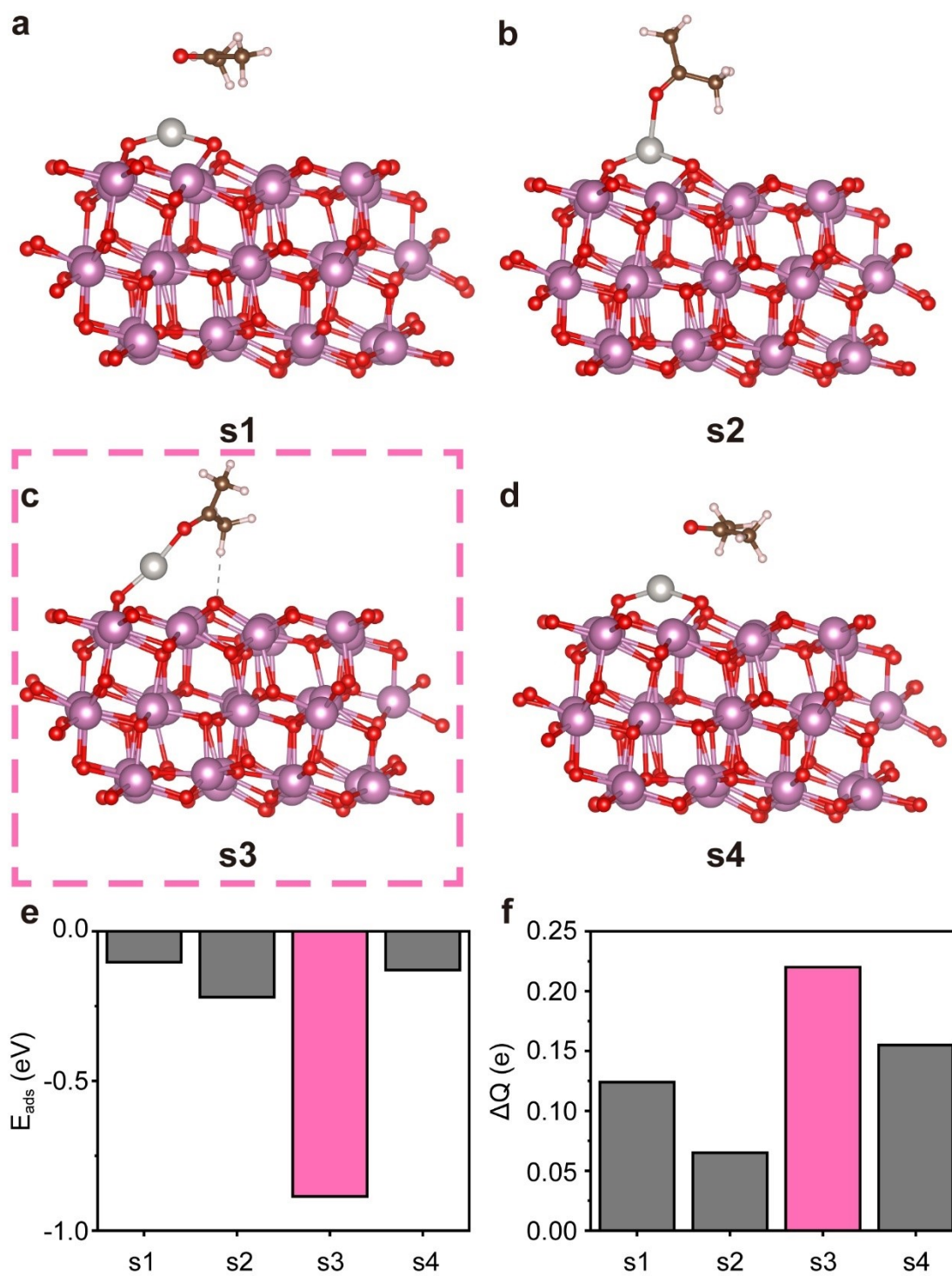


**Figure S22.** Configurations of  $\text{CH}_3\text{COCH}_3$  adsorbed onto (a, b, c, d)  $\text{Pt-In}_2\text{O}_3$ , (e, f) comparison of the calculated values of the adsorption energy and the charge transfer.

Target analyte	Metal	Configuration	Adsorption energy (eV)	$\Delta Q$ (electrons)
CH <sub>3</sub> SH	Ru	s1	-0.906	-0.061
		<b>s2</b>	<b>-1.593</b>	<b>-0.165</b>
		s3	-1.499	-0.1203
		s4	-1.007	-0.107
	Pd	s1	-0.8043	-0.172
		<b>s2</b>	<b>-1.216</b>	<b>-0.205</b>
		s3	-0.308	0.023
		s4	-1.267	-0.186
	Pt	<b>s1</b>	<b>-0.265</b>	<b>-0.1206</b>
		s2	-0.181	-0.047
		s3	-0.134	-0.060
		s4	-1.460	-0.128

**Table S2.** The computation results of the adsorption energy and the charge transfer values between CH<sub>3</sub>SH gas and metal atoms. (Bold texts indicate the optimized configuration.)

Target analyte	Metal	Configuration	Adsorption energy (eV)	$\Delta Q$ (electrons)
H <sub>2</sub> S	Ru	<b>s1</b>	<b>-0.721</b>	<b>-0.125</b>
		s2	-0.769	-0.054
		s3	-0.030	0.169
		s4	-0.732	-0.048
	Pd	<b>s1</b>	<b>-1.153</b>	<b>-0.131</b>
		s2	-1.117	-0.104
		s3	-1.124	-0.108
		s4	-1.159	-0.117
	Pt	<b>s1</b>	<b>-0.142</b>	<b>-0.045</b>
		s2	-0.093	-0.070
		s3	-0.086	0.150
		s4	-1.396	-0.011

**Table S3.** The computation results of the adsorption energy and the charge transfer values between H<sub>2</sub>S gas and metal atoms. (Bold texts indicate the optimized configuration.)

It is noted that the S atom of CH<sub>3</sub>SH has a greater electron density than that of H<sub>2</sub>S via inductive effects.<sup>1</sup> The theoretical Bader charge analyses based on the electron probability distributions can be used to estimate the electron density distribution around a molecule, through which we found that S would have a higher probability distribution in CH<sub>3</sub>SH, enabling the charge transfer. Thus, the adsorption energy and the charge transfer of CH<sub>3</sub>SH can be overestimated due to its electron-donating effects.

Target analyte	Metal	Configuration	Adsorption energy (eV)	$\Delta Q$ (electrons)
CH <sub>3</sub> COCH <sub>3</sub>	Ru	s1	-0.714	0.146
		<b>s2</b>	<b>-1.205</b>	<b>0.100</b>
		s3	-0.762	0.078
		<b>s4</b>	<b>-0.648</b>	<b>0.094</b>
	Pd	s1	-0.806	0.050
		s2	-0.567	0.114
		s3	-0.9120	0.071
		<b>s4</b>	<b>-0.944</b>	<b>0.111</b>
	Pt	s1	-0.103	0.124
		s2	-0.220	0.065
		<b>s3</b>	<b>-0.886</b>	<b>0.220</b>
		s4	-0.130	0.155

**Table S4.** The computation results of the adsorption energy and the charge transfer values between CH<sub>3</sub>SOCH<sub>3</sub> gas and metal atoms. (Bold texts indicate the optimized configuration.)

The two significant factors, adsorption energy and charge transfer were considered when optimizing the configuration of gases adsorbed on the metal atoms. For the cases of CH<sub>3</sub>SH and H<sub>2</sub>S, the final configurations were chosen based on the greater absolute values of the adsorption energy and the charge transfer. A rule of thumb in the choice of the final configuration is the greatest adsorption energy. However, if the charge transfer value, in this case, is not fair enough, the configuration with the second- or third-largest adsorption energy and the sufficiently large charge transfer was studied further. When the H atom of the gases interacts with the O atom of the oxides, colored in yellow in Table S2 and S3, the adsorption energy or the charge transfer shows smaller absolute values, supporting our optimized configurations. However, for the case of Pt, the interaction significantly reinforces the adsorption of the gas onto the oxides in addition to the adsorption on the surface of noble metals, fairly stabilizing the analyte molecules and thereby exaggerating the values of adsorption energy and charge transfer. The exaggeration, which was unlikely to be observed during sensing mechanism, made the computation results not analogous to the sensing results

of the Pt-In<sub>2</sub>O<sub>3</sub> sample, whose sensitivities against the volatile sulfur compounds were decreased by the functionalization of the Pt catalysts. Thus, we chose the configuration labeled s1, which shows no interaction between the H atom and the O atom for the Pt- In<sub>2</sub>O<sub>3</sub> sample.

Target analyte	Sample	Adsorption energy (eV)	$\Delta Q$ (electrons)	Metal-gas distance ( $\text{\AA}$ )
CH <sub>3</sub> SH	<b>0.05Ru-In<sub>2</sub>O<sub>3</sub></b>	<b>-1.593</b>	<b>-0.165</b>	<b>2.27</b>
	0.1Pd-In <sub>2</sub> O <sub>3</sub>	-1.216	-0.205	2.25
	2Pt-In <sub>2</sub> O <sub>3</sub>	-1.460	-0.128	2.76
H <sub>2</sub> S	0.05Ru-In <sub>2</sub> O <sub>3</sub>	-0.769	-0.054	2.33
	<b>0.1Pd-In<sub>2</sub>O<sub>3</sub></b>	<b>-1.153</b>	<b>-0.131</b>	<b>2.24</b>
	2Pt-In <sub>2</sub> O <sub>3</sub>	-1.396	-0.010	3.04
CH <sub>3</sub> COCH <sub>3</sub>	0.05Ru-In <sub>2</sub> O <sub>3</sub>	-1.205	0.100	2.00
	0.1Pd-In <sub>2</sub> O <sub>3</sub>	-0.944	0.111	2.03
	<b>2Pt-In<sub>2</sub>O<sub>3</sub></b>	<b>-0.886</b>	<b>0.220</b>	<b>1.99</b>

**Table S5.** The computation results of the adsorption energy, the charge transfer values and the distance between metals and gases. (Bold texts indicate the most favorable sensing materials toward each analyte.)

## Supporting Reference

1. L. S. Levitt and B. W. Levitt, *J Org Chem*, 1972, **37**, 332-&.